Associations between changes in loading pattern, deformity, and internal stresses at the foot with hammer toe during walking; a finite element approach

M. Moayedi, A. R. Arshi, M. Salehi*, M. Akrami, and R. Naemi

Abstract— Over the past decade, Finite Element (FE) modelling has been used as a method to understand the internal stresses within the diabetic foot. Foot deformities such as hammer toe have been associated with increased risk of foot ulcers in diabetic patients. Hence the aim of this study is to investigate the influence of hammer toe deformity on internal stresses during walking. A 3D finite element model of the human foot was constructed based on capturing Magnetic Resonance Imaging (MRI) of a diabetic neuropathic volunteer exhibiting hammer toe. 3D gait measurements and a multi-body musculoskeletal model for the same participant were used to define muscle forces. FE simulations were run at five different instances during the stance phase of gait. Peak plantar pressure and pressure distribution results calculated from the model showed a good agreement with the experimental measurement having less than 11% errors. Maximum von Mises internal stresses in the forefoot hard tissue were observed at the 3rd and 5th metatarsals and 4th proximal phalanx. Moreover, presence of hammer toe deformity was found to shift the location of maximum internal stresses on the soft tissue to the forefoot by changing the location of centre of pressure with internal stress more than 1.64 greater than plantar pressure. Hammer toe deformity also showed to reduce the involvement of the first phalanx in internal/external load-bearing during walking. The findings of this study support the association between changes in loading pattern, deformity, and internal stresses in the soft tissue that lead to foot ulceration**.**

Keywords
Finite element analysis, Plantar soft tissue, Diabetic Foot, Foot ulcer, Tissue Biomechanics

1. Introduction

Foot ulceration is the most frequently recognised complication in people with diabetes [1]. Epidemiology of foot ulceration and amputations showed that the prevalence of diabetic foot ulcers (DFUs) in diabetic patients could be 1.7% to 11.9% [2]. The required costs to heal the infected ulcers not requiring amputation reach ~$17,500 (in 1998 US dollars) [3]. Several factors are involved in the development of DFU [4] which foot deformity is an effective factor that causes stress concentration and additional pressure to the sole of the foot [5] and one of the high-risk factors of the deformities is hammer/claw toe [6].

Hammer-toe deformity can take place around the proximal interphalangeal joints of the lesser toe; this usually happens when the middle phalanx is flexed on the proximal one, causing hyperextension within the metatarsophalangeal joint, and a plausible flexion or extension within the distal interphalangeal joints. A hammer toe deformity manifests itself in the form of permanent angular flexion in metatarsophalangeal (MTP) joints [7]. Previous studies presented muscular imbalance, age, type of footwear, gender [8], and ineffectiveness of the intrinsic flexors [9] as common reasons for hammer toe. Moreover, simultaneous occurrence of hammer toe with neuropathy can increase the plantar pressure (PP) during walking, thus increasing the risk of ulceration [5]. For instance, in a study with 243 diabetic patients, 21% had neuropathy, and 39% had hammer toe [10]. In another study with 100 diabetic patients, 34% had neuropathy, and 32% had hammer toe [11] due to the high number of diabetic patients across the world (more than 400 million patients[12]), the number of patients with hammer toe deformity and neuropathy problems can be significant.

Mechanical trauma resulting from excess mechanical loading is considered a cause of DFU [13-17]. Thus, several studies focused on assessing the plantar pressure during walking [18-20]. In 2003, model developed by Gelofen [21] showed that internal stresses could be several times greater than the plantar pressure. However, unlike plantar pressure that can be measured using pressure sensors, the internal stresses cannot be measured experimentally and require finite element modelling approaches. The geometry of the FE model is composed based on segmentation and reconstruction of medical images (Computed Tomography (CT) images, Magnetic Resonance Imaging (MRI), and X-ray images; (X-ray is not used nowadays)) [22-30]. In recent years, the musculoskeletal model with finite element modelling (FEM) was used to increase the accuracy of prediction results of numerical models, so in addition to the boundary conditions gathered from gait analysis, muscle forces are also applied to the model [31-33]. Despite the existence of such models, there is a scarcity of specific models in which hammer toe

M. Moayedi and M. Salehi are with the Department of Mechanical Engineering, Amirkabir University of Technology, Iran (e-mail:{m.moayedi, msalehi}@aut.ac.ir)

A. R. Arshi is with Biomechanics and Sports Engineering Groups, Biomedical Engineering Department, Amirkabir University of Technology, Iran (e-mail: arshi@aut.ac.ir)

M. Akrami is with Department of Engineering, College of Engineering, Mathematics, and Physical Sciences, University of Exeter, U.K (M.Akrami@exeter.ac.uk)

R. Naemi is with the Centre for Biomechanics and Rehabilitation Technologies, Staffordshire University, UK (e-mail: r.naemi@staffs.ac.uk).

* Corresponding author

deformity is constructed and the effect of deformity on the internal stresses in both soft tissue and bones are investigated. The aim of this study is to investigate the effects of hammer toe on the distribution of internal and external stresses in both the soft tissue and the bone during walking.

2. Method

A diabetic subject (male; age: 53 years; body mass index (BMI): 34 kg/m^2) with neuropathy and hammer toes abnormalities in the left foot and with healthy right foot, participated in this study following informed consent. A 3D FEM of the left foot was developed using person-specific MRI and gait analysis. Fig. 1 shows four slices of MRI images in sagittal view and as shown in this figure, the proximal phalanges have deviated from normal to different degrees. The 4th and the 5th toe are closer to normal form and have less deviation compared with 2nd and 3rd phalanges. Muscle forces were derived based on the musculoskeletal model (MSM) along with the 3D ground reaction forces (GRFs), which were added to the model as boundary conditions. For validation, plantar pressure and its distribution were compared in five phases of walking and at the end, the effects of hammer toe deformity on the biomechanics of the foot were discussed. The steps required to achieve a complete model were taken as follows: 1) MRI imaging of the foot. 2) Integrated 3D motion capture (gait analysis). 3) Calculation of muscle forces with musculoskeletal modelling. 4) Conversion of MRI images into a three-dimensional model with segmentation in Mimics software and 5) Computation of stresses and PP in soft tissues and bones through use of FEMs.

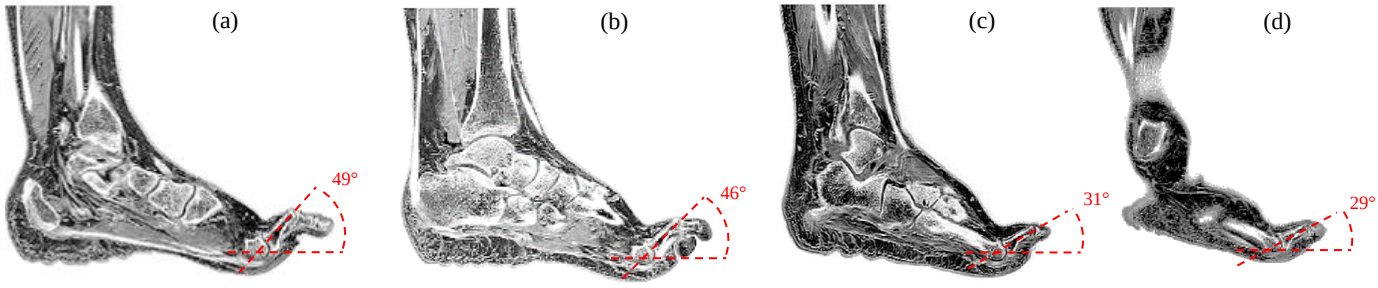

Fig. 1. Comparison of approximate proximal phalanges deviation visible in the MRI pictures in sagittal medial view of the left foot. a) 2nd toe at approximately 49° has the maximum deviation, b) 3rd toe with approximately 46° deviation, c) 4th toe with approximately 31° deviation, d) 5th toe with approximately 29° deviation

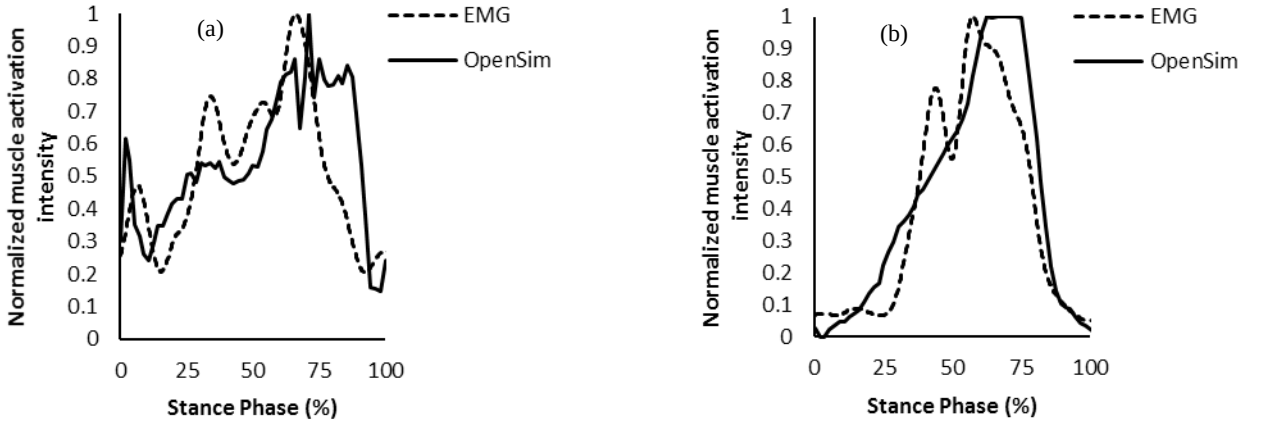

Fig. 2. Muscle activation intensity which normalised in the period of stance phase; (a) tibialis anterior, this shows a good agreement between EMG and OpenSim results with Root-Mean Square Error (RMSE) 0.19 and (b) medial gastrocnemius, this also presents a reasonable assent between EMG and OpenSim results with RMSE 0.17

3. Gait Measurement

Three-dimensional gait analysis was carried out on the same participant. 24 Markers were positioned on the lower limb and trunk based on the Vicon Plug-In Gait marker placement recommendations [34]. In addition, 14 extra markers were positioned on the lower extremities at the following anatomical landmarks;

left and right medial femoral condyle, left and right greater trochanteric [35], left and right first metatarsal head, left and right fifth metatarsal head, left and right anterior tibia, at the half of part length, left and right anterior thigh, at the half of part length [36, 37], left and right dorsal surface of the second metatarso-cuneiform joint [38]. The placement of the 38 markers are shown in Appendix A. Gait analysis was carried out by 10 infrared cameras motion capture system (Vicon, Oxford, UK) sampling at 100 Hz, and two force plates (Kistler, Winterthur, Switzerland) were used to record the GRFs at 100 Hz and one pressure pad system (Payatek, , Tehran, Iran) was used to collect the pressure distribution of the foot. For validation of muscle forces and intensity of muscle activation, a six-channel surface electromyography (EMG) system (Myon, Schwarzenberg, Switzerland) was placed based on SENIAM guidelines [39, 40]. EMG data was processed with a five-step approach. The data passed through a fifth order Butterworth high-pass filter at 30 Hz, demeaned, and full wave rectified. Then the outputs were low-pass

filtered by a fourth order Butterworth filter at 5Hz, and subsequently normalised against highest activity [41]. Kinematic data, GRFs, and muscle activation signals were collected synchronously using Nexus software (Vicon, Oxford, UK).

The muscle activities of six major muscles: soleus, lateral gastrocnemius, medial gastrocnemius, tibialis posterior, tibialis anterior, and peroneus longus were acquired. The participant was asked to walk barefoot at normal walking speed along the walkway. Several trials were repeated to ensure repeatability of the results and gait pattern. The trajectory data of markers, muscle activation signals, and GRFs were collected, used to obtain muscle forces, boundary conditions, and validation of FE results. In addition to the dynamic trials, data of a static trial was collected, and used for scaling of the musculoskeletal model.

4. Muscle force estimation

OpenSim software [42] has several generic musculoskeletal models that can be used for various purposes, such as predicting muscle forces. In this study, the 'gait 2392' model [42] was deployed based on previous studies [31-33]. This comprehensive model consists of 10 rigid bodies with 23 degrees of freedom (DOF) and 92 musculotendon actuators. Scaling of the generic model was performed using the static trial data (position of markers and body mass of participant). The lower limb contains seven segments: femur, talus, pelvis, tibia/fibula, patella, foot (metatarsals, cuneiforms, cuboid, navicular, and calcaneus) and toes. All the muscle forces of the leg were obtained by static optimization during walking. For validation purposes, simulated muscle activation of six intended muscles (soleus, lateral gastrocnemius, medial gastrocnemius, tibialis posterior, tibialis anterior, and peroneus longus) during the stance phase of gait were compared against the corresponding muscle activities derived experimentally.

Comparing the normalised muscle activation, the intensity results of EMG and OpenSim indicate a reasonable agreement (with RMSE of 0.19 and 0.17 for tibialis anterior and medial gastrocnemius) of the modelled muscle force estimations against the real forces. The comparison for the results of lateral gastrocnemius and tibialis anterior muscle activation can be seen in Fig. 2 showing a good agreement.

5. Finite Element Modeling

The 3D model of the foot consisted of soft tissue (skin, fat, muscles, and tendons), hard tissues (bones), and the Achilles tendon, which were constructed by segmenting the MRI images using Mimics software (Materialise, Leuven, Belgium). The left foot MRI was acquired in an unloaded condition using a 1.5 Tesla MRI scan (Philips Ingenia, spacing between slices: 0.5 mm and slice thickness: 1 mm, sequence 3D mDion Te Hr, TE/TR 9/29). The angle between the foot and leg were kept at approximately 90 degrees by pads and pillows to improve the accuracy of the 3D reconstructions. The obtained models were polished with the help of 3-Matic software (Materialise, Leuven, Belgium) to avoid causing problems in the meshing process and to avoid sharp corners. Thirty hard tissue structures were included as follows (navicular, talus, 3 cuneiforms, calcaneus, cuboid, 5 metatarsals, medial and lateral sesamoids, 14 phalanges, and the distal parts of the tibia and fibula). To enhance the accuracy of modelling and enable frictionless movement of the bones, 74 cartilage layers were added to the model for 37 pairs of articulations among 30 bones. Surface-to-surface frictionless contact was used between cartilage layers.

All parts (30 bones, one bulk soft tissue, one Achilles tendon, and the cartilage parts) were imported to ABAQUS software (SIMULIA, Providence, USA) to perform and run the finite element analysis. Due to the difficulties in detecting the ligaments in MRI, these were manually added to the model and located based on the anatomical landmarks, and also for plantar fascia [43]. In total 2174 truss elements were used to represent the major ligaments in the foot. Due to the nature of the ligaments, the properties of these elements were defined as tension only [44]. The plantar fascia was modelled by connecting the proximal phalanges of the toes to the medial calcaneal tubercle. The Achilles tendon as a separate 3D part was placed over the calcaneus and tied to it (see Fig. 3). The muscle forces from soleus, lateral, and medial gastrocnemius, were introduced to the Achilles tendon. All the bones, ligaments, Achilles tendon, and cartilages were embedded in a 3D bulk of soft tissues that encapsulated other foot components (see Fig. 3). To create the connection conditions of the area between the proximal and distal, the upper part of the fibula, tibia, and bulk of the soft tissue were considered to be fixed in all DOF. The ground was added to the model as a 3D solid plate. The interaction between the ground plate and the foot plantar surface was considered with a frictional coefficient of friction of 0.6

Table 1. Material properties [47, 48] and element types of different parts of the model

Components	Young's modulus (MPa)	Poisson's ratio	Cross section (mm²)	Element Type
Hard tissue	7300	0.3	--	Tetrahedral
Ligament	260	--	18.4	Truss
Cartilage	1	0.4	--	Tetrahedral
Plantar fascia	350	--	290.7	Truss
Ground	17000	0.1	--	Linear hexahedral
Achilles	816	3.0	--	Tetrahedral
Encapsulated soft tissue	Hyperelastic (second-order polynomial strain energy potential equation, C_{10} = 0.08556 Nmm^{-2},C_{01} = -0.05841 Nmm^{-2}, C_{20} = 0.03900 Nmm^{-2}, C_{11} = -0.02319 Nmm^{-2}, C_{02} = 0.00851 Nmm^{-2},D_1 = 3.65273 mm^2N^{-1}, D_2 = 0.0000 mm^2N^{-1})			Tetrahedral

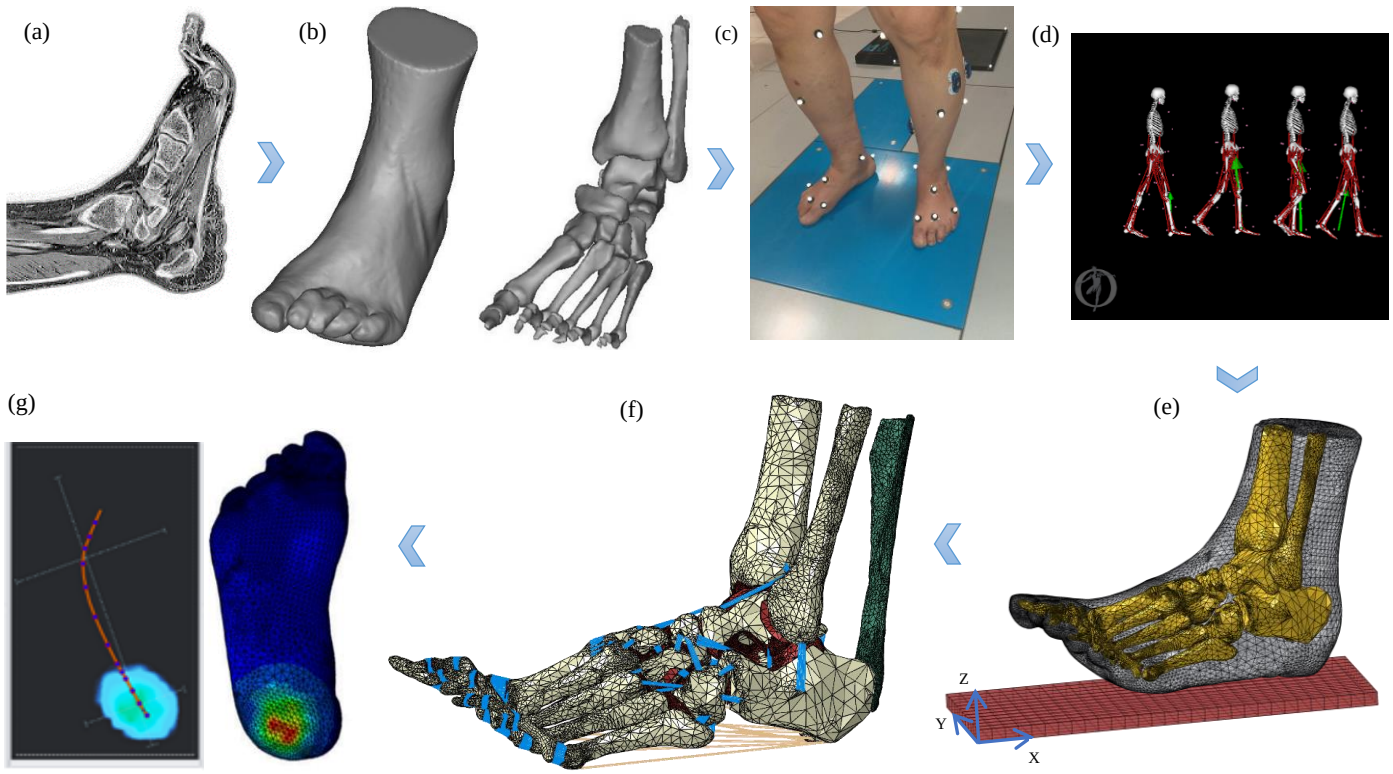

Fig. 3. An Overview of the process steps (a) MRI imaging (b) 3D soft and hard tissues constructed by segmentation of the MRI images in Mimics software (c) Marker set, Gait analysis, and EMG test (d) Muscle force estimation by musculoskeletal modelling using Mimics software. In order to represent walking in OpenSim modeling, four frames from the gait sequence were selected and shown (e) Importing 3D foot model (bony structure and soft tissue bulk) into ABAQUS and applying the boundary condition to the model (f) Adding the cartilage and ligaments to the 3D model (g) Running the model (shown as the mirrored plantar view of the left foot) and comparing the plantar pressure results of the finite element simulation with those of the test.

Table 2. Muscle forces obtained from OpenSim in five phases of walking

Muscle forces (N)	Gait events				
	Heel strike (%10)	Early stance (%25)	Mid-stance (%50)	Late stance (%75)	Toe off (%90)
Medial gastrocnemius	58.24	249.72	1559.73	1415.94	263.23
Lateral gastrocnemius	19.04	142.53	482.93	558.72	92.76
Soleus	0.15	500.4	103.95	1521.64	1326.36
Tibialis posterior	87.34	473.66	745.02	759.64	387.45
Tibialis anterior	182.35	193.53	242.24	301.07	236.87
Peroneus longus	0.16	0.021	0.022	0.006	0.037

based on a previous study [45]. The GRFs that were measured at a representative walking trial were then induced to the ground plate at the COP, based on COP's location relative to the position of the anatomical landmarks.

Six force vectors that were calculated from MSM were used as the muscle forces in the FE simulation and with simplification, from these forces, three were applied directly to the points on the Achilles tendon and three others were applied to the bones all in the direction of each six muscle forces [46]. As it is not possible to find the properties of living tissues with in vivo testing, all parts of the foot (hard tissues, ligaments, and plantar soft tissue) and ground plate were considered as isotropic and homogeneous based on the literature [47, 48]. Table 1 presents the material properties of all foot components and ground plate. The mesh was determined with 664,304 elements and 299,067 nodes by a mesh sensitivity study until the calculated stress deviations were less than 5%. Computational time was on average, 17 hours with a processor: Core™ i7-6700 CPU @ 3.4 GHz.

Table 3. Measured 3D foot orientation angles (in degrees).

	Heel strike	Early stance	Mid-stance	Late stance	Toe off
Roll (α) ° (Rotation around x axis)	10.82	9.49	6.21	3.04	7.59
Pitch (β) ° (Rotation around y axis)	5.58	-2.13	-3.26	-6.81	-34
Yaw (γ) ° (Rotation around z axis)	16.08	14.01	13.23	13.76	14.07

5.1. Finite element simulations of walking

For the purpose of this study, walking was simulated as a series of static conditions. While dynamic simulation may enhance the precision of FE estimations, it requires significantly higher computational processing power. The walking step can be considered as several static phases and this can save the computational cost and time. FE simulations were performed at five gait events (heel strike, early stance, mid-stance, late stance, and toe off). During each event, boundary conditions were fully fixed at superior surfaces of

the fibula, tibia, and bulk soft tissue [49]. The GRFs collected from the force plates were applied to the ground plate at the COP. Based on the fixed global coordinate system on the ground, three angles (α, β, γ) of the foot during the gait cycle were introduced for each five stance events representing the gait patterns. Muscle forces were assigned for each gait phase at their anatomical insertion locations along the 3D muscle force vectors determined from the OpenSim model. The muscle forces are listed in table 2, and also 3D GRFs are plotted during a step in fig. 4, used to describe the loading scenarios in the FE simulations. The 3D foot orientation angles (α, β, γ) are given in table 3.

6. Validation

For validation of the FE results, plantar pressure was compared against the corresponding plantar pressure data measured during walking. Fig. 5 shows this comparison across different regions of the foot. The peak plantar pressure distribution showed a good agreement at all 5 stance phases of walking.

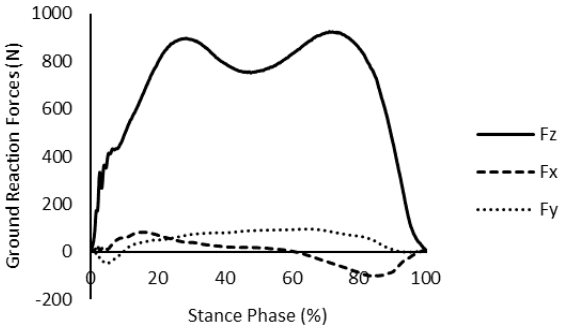

Fig. 4. Measured 3D ground reaction forces during walking.

7. Result

Plantar pressure of left foot was obtained in the range of 0 to 850 (KPa) from experimental test and in the range of 0 to 922 (KPa) from FE estimation, which in this respect, these are almost 8% different from each other (see fig. 5). The peak PP was estimated with the error range of 4% to 11% in comparison to experimental results; the highest error occurred in late stance and the lowest error occurred in early stance.

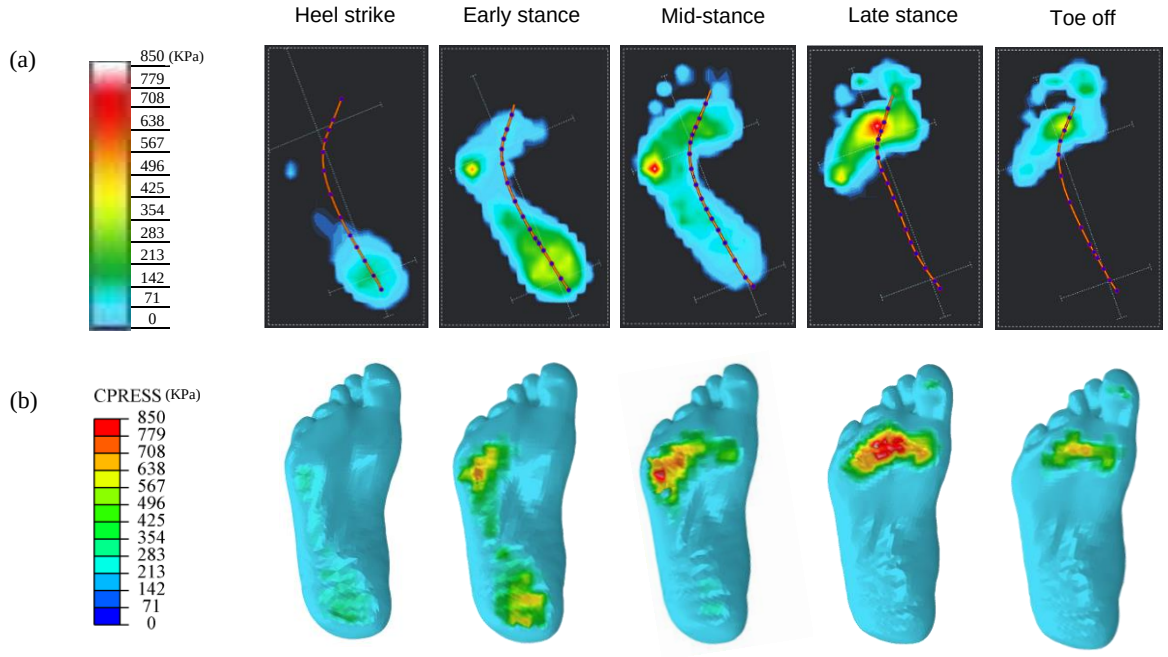

Fig. 5. Result comparison of plantar pressure (a) data recorded experimentally (b) F.E. simulation results at five different instances during the stance phase of walking trial (shown as the mirrored plantar view of the left foot). Error of maximum PP between a and b, ~8 % in heel strike, ~4 % in early stance, ~5 % in mid-stance, ~7 % in late stance and ~11 % in toe off

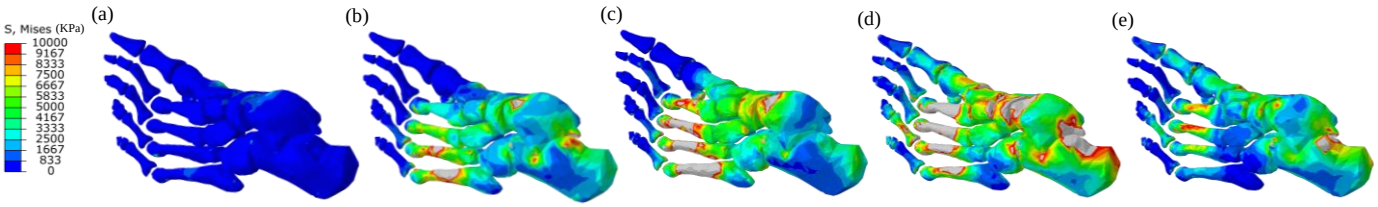

Fig. 6. Internal stresses in bones at five walking events: (a) Heel strike (b) Early stance, (c) Mid-stance, (d) Late stance and (e) Toe off. Light grey colour shows the von Mises higher than 10 MPa. For getting an overview of the full stress distribution for each phase of gait please consult the supplementary material in Appendix B.

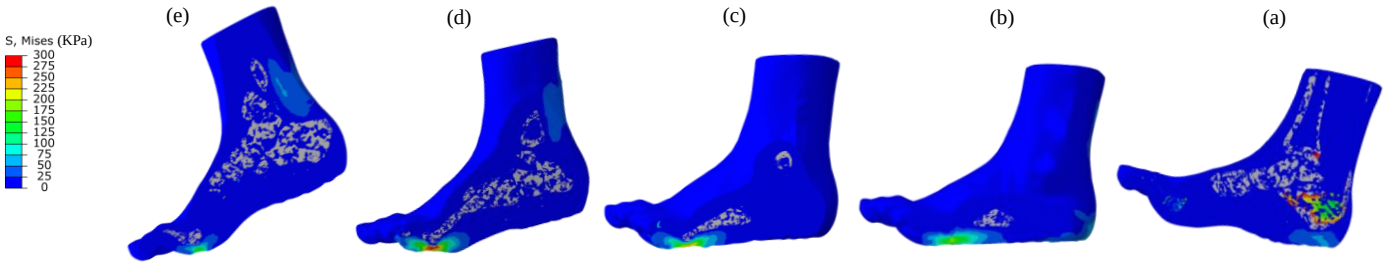

Fig. 7. Soft tissue internal von Mises stress distribution on sagittal planes where the maximum stresses occur at five walking events: (a) Heel strike (b) Early stance, (c) Mid-stance, (d) Late stance and (e) Toe off. Light grey colour showed the bony structures with the internal von Mises stresses higher than 300 KPa.

Fig. 6 shows stress distribution in the bony structures. Looking at the standpoint of internal stresses, it is evident that the maximum stresses in the forefoot hard tissue happen at the 4th proximal phalanx and also the 3rd metatarsal, furthermore 4th and 5th metatarsals were in a high level of higher stress-time integral, which these phalanges have relatively less deformity in comparison with the 2nd and 3rd phalanges.

Fig. 7 shows internal von Mises stress distribution at the soft tissue. As shown in this figure, maximum stress could occur at the internal region of soft tissue and the difference between plantar pressure and internal stress may be significant. Results showed that maximum von Mises stress in the soft tissue occurs at sub-metatarsal heads (sub-MTHs) and heel-pad, with the highest registered in the late stance at 3rd sub-MTH. As mentioned in the method section, the participant had hammer toe deformity only in his left foot and the right foot was healthy. By comparing the results of peak PP distribution in the right and left foot, it is obvious that the maximum pressure in the left foot (850 KPa) was 37% higher than the peak PP in the right foot (620 KPa) and the deformity of the phalanges caused a reduction in the involvement of the rear-foot during walking. Therefore, the presence of hammer toe deformity, in addition to a reduction of the duration of weight-bearing in the rear foot, causes a stress concentration in the forefoot, and this can increase the risk of ulcers and can also change the forces and moments induced to joints.

8. Discussion

Diabetic neuropathy causes muscle weakness and deformities in the foot. The presence of these deformities will increase the risk of ulcers. One of the common deformities in diabetic foot is hammer toe. Prevention of diabetic foot ulcers is vital for people with these conditions. However despite various studies in foot simulations, the effect of hammer toe on internal stress distribution in both the soft tissue and the bone has not been investigated. To achieve this, 3D foot-ankle model inclusive of 30 bony tissues, a bulk soft tissue, major ligaments consisting of 2174 truss elements, and 74 layers of cartilage were constructed. The accuracy of the model was further improved by including ligaments and cartilage. In addition to applying GRFs as boundary conditions, in order to improve the precision of the FE results, six muscle forces were estimated based on a musculoskeletal model that enables the inclusion of the muscle forces on the bones. Validation of estimated muscle forces was done by comparing the EMG signals and estimated muscle activation intensity [50, 51]. This indicated a very similar activation pattern and good agreement between the estimated muscle activation intensity based on the models against the measured EMG signals.

Maximum von Mises stresses in the soft tissue were found at the heel during heel strike, 5th sub-MTH during early stance and mid-stance, 3rd sub-MTH during late stance and 2nd sub-MTH during toe off, and also maximum PP occurred at 5th and 2nd sub-MTH. Previous studies showed that the metatarsal heads and the heel are usual locations of DFU and the location of ulcer also depends on the foot deformity [1, 53-56]. While it was previously mentioned that in addition to the superficial injuries, subcutaneous injuries should also be considered as a cause of ulceration [1], Armstrong and Lavery [55] showed hallux and first MTH are areas of high plantar pressures and are more vulnerable to be sites of plantar ulcers in neuropathic foot. In the present study, the most common sites for the highest peak pressure were 2nd, 3rd, and 5th sub-MTHs. However, the peak of the von Mises stresses (internal stress) occurred at 3rd sub-MTH soft tissue, which confirms early suggestion by Bus et al. [57] and it is in contrast with the results from healthy foot [30]. The results of the current study indicate the contribution of hammer toe in increasing PP and internal stress at the plantar soft tissue at the MTHs and indicating the higher risk of DFU in these areas [52].

The maximum von Mises stresses (internal stress) for bony structures were observed at the 3rd and 5th metatarsals and the peak of stresses occurred at the 5th metatarsal. Overall, more deformities in the middle of the foot (2nd and 3rd phalanx) caused the first toe to play a lesser role in withstanding the internal stresses and in a long time, it can have a negative effect on the normal form of the foot, ankle, and also other lower limb joint functions. Moreover, the internal stresses on the bony structure showed that the parts of the foot with hammer toe, which are in a healthier conditions, will be under more significant stresses and this issue can provide conditions for deformity in those parts of the foot. The results of this study can also indicate that the stress-time integral is at a higher level at the fourth and fifth metatarsals compared with the other metatarsals and this can cause future deformity in two phalanges; That is in line with to what was reported by Wong et al. [33], which indicated that a reduction in load-carrying capacity can be an effective factor in the development of foot deformities.

The present results showed peak PP in the foot with

deformity could be 1.37 times higher than a foot without deformity, which is in line with the experimental results presented in a previous study [57]. The results of this study in which a lower rearfoot loading in the foot with hammer toe deformity was observed is in line with previous findings [58]. In that study also a lower peak plantar pressure was observed in the rearfoot of group with diabetic hammer and clawed toe deformities versus heathy controls [58]. Also similar to the previous findings, in our study the forefoot deformity seem to be associated with a promotion in forefoot loading and stress time integral [57, 59]. In fact in a previous study a lower maximum force and peak plantar pressure were observed in patients with Hallux Valgus [60]. This can be the result of changes in the gait and these results suggest that the rearfoot may have an important role in the aetiology of hammer toe deformity, where further investigations are warranted future.

Moreover, the FE results indicated that internal stresses at the soft tissue could be 1.64 times greater than the plantar surface stresses. Thus, a diabetic foot deformity should be examined more carefully to avoid either surface or internal overload that can lead to ulceration especially at the plantar soft tissue of the sub-MTHs.

The present study is patient-specific and if the geometry of the foot, type, and position of deformity change, the results might differ. However, the results clearly illustrate that the existence of deformities such as hammer toe in the foot can affect the distribution of stresses in both hard and soft tissues; this is important for preventing both diabetic foot ulcers and progressive foot deformities that can lead to increase in the plantar soft tissue stress.

9. Conclusion

In this study, a 3D FE model of hammer toe foot was developed to investigate the internal stress in soft and bony tissues during different stance phases of the gait. This study showed hammer toe deformity could raise the risk of foot ulcers by increasing the internal stresses on the plantar soft tissue. Furthermore, the increased stresses on the bones of the foot create a progressive pattern of excessive loads, which can further increase the deformity. These support the association between changes in load-bearing pattern, deformity, and internal stresses in the tissue that can lead to an increase in the risk of diabetic foot ulceration.

Acknowledgments

The authors would like to thank Mr. Akbar Hoshyarkohi and Pardis Noor Medical Imaging Center, Tehran, for their technical support in MRI imaging. We also thank the Structure and Motion Lab, Movafaghian research center, Tehran, to help with the gait analysis.

References

[1] D. G. Armstrong, A. J. Boulton, and S.A. Bus, "Diabetic foot ulcers and their recurrence," New England Journal of Medicine, vol. 376, no. 24, pp. 2367-2375, Jun 2017, https://doi.org/10.1056/NEJMra1615439.

[2] A. J. Boulton, L. Vileikyte, G. Ragnarson-Tennvall, and J. Apelqvist, "The global burden of diabetic foot disease," The Lancet, vol. 366, no. 9498, pp. 1719-1724, Nov 2005, https://doi.org/10.1016/S0140-6736(05)67698-2.

[3] G. Ragnarson Tennvall, and J. Apelqvist, "Health-economic consequences of diabetic foot lesions," Clinical Infectious Diseases, vol. 39, no. Supplement_2, pp. S132-S139, Aug 2004, https://doi.org/10.1086/383275.

[4] J. Tulloch, R. Zamani, and M. Akrami, "Machine learning in the prevention, diagnosis and management of diabetic foot ulcers: A systematic review," IEEE Access, vol. 8, pp. 198977-19900, Nov 2020, https://doi.org/10.1109/ACCESS.2020.3035327.

[5] U. H. Tang, R. Zügner, V. Lisovskaja, J. Karlsson, K. Hagberg, and R. Tranberg, "Foot deformities, function in the lower extremities, and plantar pressure in patients with diabetes at high risk to develop foot ulcers," Diabetic foot & ankle, vol. 6, no. 1, pp. 27593, Jan 2015, https://doi.org/10.3402/dfa.v6.27593.

[6] E. J. Boyko, J. H. Ahroni, V. Stensel, R. C. Forsberg, D. R. Davignon, and D. G. Smith, "A prospective study of risk factors for diabetic foot ulcer. The Seattle Diabetic Foot Study," *Diabetes Care*, vol. 22, no. 7, pp. 1036–1042, Jul 1999, https://doi.org/10.2337/diacare.22.7.1036.

[7] M. J. Coughlin, "Lesser-Toe Abnormalities," *The Journal of Bone & Joint Surgery*, vol. 84, no. 8, pp. 1446–1469, Aug. 2002, https://doi.org/10.2106/00004623-200208000-00023.

[8] M. Scheck, "Etiology of acquired hammertoe deformity," Clinical Orthopaedics and Related Research, vol. 123, pp.63-69, Mar 1977.

[9] R. G. Taylor, "The Treatment of Claw Toes By Multiple Transfers of Flexor into Extensor Tendons," *The Journal of Bone and Joint Surgery. British volume*, vol. 33-B, no. 4, pp. 539–542, Nov. 1951, https://doi.org/10.1302/0301-620x.33b4.539.

[10] C. Formosa, A. Gatt, and N. Chockalingam, "The importance of clinical biomechanical assessment of foot deformity and joint mobility in people living with type-2 diabetes within a primary care setting," *Primary Care Diabetes*, vol. 7, no. 1, pp. 45–50, Apr. 2013, https://doi.org/10.1016/j.pcd.2012.12.003.

[11] J. J. Holewski, K. M. Moss, R. M. Stess, P. M. Graf, and C. Grunfeld, "Prevalence of foot pathology and lower extremity complications in a diabetic outpatient clinic," *J Rehabil Res Dev*, vol. 26, no. 3, pp. 35-44, 1989.

[12] P. Saeedi, I. Petersohn, P. Salpea, B. Malanda, S. Karuranga, N. Unwin, S. Colagiuri, L. Guariguata, A. A. Motala, K. Ogurtsova, J. E. Shaw, D. Bright, and R. Williams, "Global and regional diabetes prevalence estimates for 2019 and projections for 2030 and 2045: Results from the International Diabetes Federation Diabetes Atlas, 9th edition," *Diabetes Research and Clinical Practice*, vol. 157, p. 107843, Nov. 2019, https://doi.org/10.1016/j.diabres.2019.107843.

[13] B. H. M. Tan, A. Nather, and V. David, (2008). "Biomechanics of the foot," in *Diabetic Foot Problems*, pp. 67-75, 2008, https://doi.org/10.1142/9789812791535_0006.

[14] C. M. Van Schie, "A review of the biomechanics of the diabetic foot," *The international journal of lower extremity wounds*, vol. 4, no. 3, pp. 160-170, Sep. 2005, https://doi.org/10.1177/1534734605280587 .

[15] C. H. van Schie, and A. J. Boulton, "Biomechanics of the diabetic foot: the road to foot ulceration," In *The diabetic foot*, Totowa, NJ: Humana Press, 2002, pp. 147-161.

[16] P. R. Cavanagh, J. S. Ulbrecht, and G. M. Caputo, "New developments in the biomechanics of the diabetic foot," *Diabetes/Metabolism Research and Reviews*, vol. 16, no. S1, Sep. 2000. https://doi.org/10.1002/1520-7560(200009/10)16:1+<::AID-DMRR130>3.0.CO;2-Z.

[17] J. Bevans, "Biomechanics and plantar ulcers in diabetes," *The Foot*, vol. 2, no. 3, pp. 166–172, Sep. 1992. https://doi.org/10.1016/0958-2592(92)90067-y.

[18] T. Duckworth, A. Boulton, R. Betts, C. Franks, and J. Ward, "Plantar pressure measurements and the prevention of ulceration in the diabetic foot," *The Journal of Bone and Joint Surgery. British volume*, vol. 67-B, no. 1, pp. 79–85, Jan. 1985, https://doi.org/10.1302/0301-620x.67b1.3968150.

[19] R. G. Frykberg, L. A. Lavery, H. Pham, C. Harvey, L. Harkless, and A. Veves, "Role of Neuropathy and High Foot Pressures in Diabetic Foot Ulceration," *Diabetes Care*, vol. 21, no. 10, pp. 1714–1719, Oct. 1998, https://doi.org/10.2337/diacare.21.10.1714.

[20] A. Caselli, H. Pham, J. M. Giurini, D. G. Armstrong, and A. Veves, "The Forefoot-to-Rearfoot Plantar Pressure Ratio Is Increased in Severe Diabetic Neuropathy and Can Predict Foot Ulceration," *Diabetes Care*, vol. 25, no. 6, pp. 1066–1071, Jun. 2002, https://doi.org/10.2337/diacare.25.6.1066.

[21] A. Gefen, "Plantar soft tissue loading under the medial metatarsals in the standing diabetic foot," *Medical engineering & physics*, vol. 25, no. 6, pp. 491-499, Jul. 2003, https://doi.org/10.1016/s1350-4533(03)00029-8.

[22] Z. Wang, K. Imai, M. Kido, K. Ikoma, and S. Hirai, "A finite element model of flatfoot (Pes Planus) for improving surgical plan," *2014 36th Annual International Conference of the IEEE Engineering in Medicine and Biology Society*, Aug. 2014, https://doi.org/10.1109/embc.2014.6943723.

[23] V. Isvilanonda, E. Dengler, J. M. Iaquinto, B. J. Sangeorzan, and W. R. Ledoux, "Finite element analysis of the foot: Model validation and comparison between two common treatments of the clawed hallux deformity," *Clinical Biomechanics*, vol. 27, no. 8, pp. 837–844, Oct. 2012, https://doi.org/10.1016/j.clinbiomech.2012.05.005.

[24] P.-C. Sun, S.-L. Shih, Y.-L. Chen, Y.-C. Hsu, R.-C. Yang, and C.-S. Chen, "Biomechanical analysis of foot with different foot arch heights: a finite element analysis," *Computer Methods in Biomechanics and Biomedical Engineering*, vol. 15, no. 6, pp. 563–569, Jun. 2012, https://doi.org/10.1080/10255842.2010.550165.

[25] E. Brilakis, E. Kaselouris, F. Xypnitos, C. G. Provatidis, and N. Efstathopoulos, "Effects of Foot Posture on Fifth Metatarsal Fracture Healing: A Finite Element Study," *The Journal of Foot and Ankle Surgery*, vol. 51, no. 6, pp. 720–728, Nov. 2012, https://doi.org/10.1053/j.jfas.2012.08.006.

[26] K. Tao, D. Wang, C. Wang, X. Wang, A. Liu, C. J. Nester, and D. Howard, "An In Vivo Experimental Validation of a Computational Model of Human Foot," *Journal of Bionic Engineering*, vol. 6, no. 4, pp. 387–397, Dec. 2009, https://doi.org/10.1016/s1672-6529(08)60138-9.

[27] T.-X. Qiu, E.-C. Teo, Y.-B. Yan, and W. Lei, "Finite element modeling of a 3D coupled foot–boot model," *Medical Engineering & Physics*, vol. 33, no. 10, pp. 1228–1233, Dec. 2011, https://doi.org/10.1016/j.medengphy.2011.05.012.

[28] M. A. Ellison, M. Akrami, J. Fulford, A. A. Javadi, and H. M. Rice, "Three dimensional finite element modelling of metatarsal stresses during running," *Journal of Medical Engineering & Technology*, vol. 44, no. 7, pp. 368–377, Aug. 2020, https://doi.org/10.1080/03091902.2020.1799092.

[29] S. Li, Y. Zhang, Y. Gu, and J. Ren, "Stress distribution of metatarsals during forefoot strike versus rearfoot strike: A finite element study," *Computers in biology and medicine*, vol. 91, pp. 38-46, Dec. 2017, https://doi.org/10.1016/j.compbiomed.2017.09.018.

[30] Y. Zhang, J. Awrejcewicz, O. Szymanowska, S. Shen, X. Zhao, J.S. Baker, and Y. Gu, "Effects of severe hallux valgus on metatarsal stress and the metatarsophalangeal loading during balanced standing: A finite element analysis," *Computers in biology and medicine*, vol. 97, pp. 1-7, Jun. 2018, https://doi.org/10.1016/j.compbiomed.2018.04.010.

[31] M. Akrami, Z. Qian, Z. Zou, D. Howard, C. J. Nester, and L. Ren, "Subject-specific finite element modelling of the human foot complex during walking: sensitivity analysis of material properties, boundary and loading conditions," *Biomechanics and Modeling in Mechanobiology*, vol. 17, no. 2, pp. 559–576, Nov. 2017, https://doi.org/10.1007/s10237-017-0978-3.

[32] A. Scarton, A. Guiotto, T. Malaquias, F. Spolaor, G. Sinigaglia, C. Cobelli, I. Jonkers, and Z. Sawacha, "A methodological framework for detecting ulcers' risk in diabetic foot subjects by combining gait analysis, a new musculoskeletal foot model and a foot finite element model," *Gait & Posture*, vol. 60, pp. 279–285, Feb. 2018, https://doi.org/10.1016/j.gaitpost.2017.08.036.

[33] D. W.-C. Wong, Y. Wang, T. L.-W. Chen, F. Yan, Y. Peng, Q. Tan, M. Ni, A. K.-L. Leung, and M. Zhang, "Finite Element Analysis of Generalized Ligament Laxity on the Deterioration of Hallux Valgus Deformity (Bunion)," *Frontiers in Bioengineering and Biotechnology*, vol. 8, Sep. 2020, https://doi.org/10.3389/fbioe.2020.571192.

[34] Docs.vicon.com. 2021. *PDF Downloads For Vicon Nexus - Nexus 2.11 Documentation - Vicon Documentation*. [online] Available at: <https://docs.vicon.com/display/Nexus211/PDF+downloads+for+Vicon+Nexus> [Accessed 14 January 2021].

[35] F. Stief, H. Böhm, K. Michel, A. Schwirtz, and L. Döderlein, "Reliability and accuracy in three-dimensional gait analysis: a comparison of two lower body protocols," *Journal of applied biomechanics*, vol. 29, no. 1, 2013, https://doi.org/10.1123/jab.29.1.105.

[36] P. J. Renaud, "Three-dimensional kinematics of the lower limbs during ice hockey skating starts on the ice surface," McGill University (Canada), 2016.

[37] E. Flux, M. M. van der Krogt, P. Cappa, M. Petrarca, K. Desloovere, and J. Harlaar, "The Human Body Model versus conventional gait models for kinematic gait analysis in children with cerebral palsy," *Human movement science*, vol. 70, p. 102585, 2020, https://doi.org/10.1016/j.humov.2020.102585.

[38] A. Leardini, M. G. Benedetti, L. Berti, D. Bettinelli, R. Nativo, and S. Giannini, "Rear-foot, mid-foot and fore-foot motion during the stance phase of gait," *Gait & posture*, vol. 25, no. 13, pp.453-462, Mar. 2007, https://doi.org/10.1016/j.gaitpost.2006.05.017.

[39] H. J. Hermens, B. Freriks, R. Merletti, D. Stegeman, J. Blok, G. Rau, C. Disselhorst-Klug, and G. Hägg, "European recommendations for surface electromyography," *Roessingh research and development*, vol. 8, no. 2, pp.13-54, 1999.

[40] S. McGill, D. Juker, and P. Kropf, "Appropriately placed surface EMG electrodes reflect deep muscle activity (psoas, quadratus lumborum, abdominal wall) in the lumbar spine," *Journal of biomechanics*, vol. 29, no. 11, pp. 1503-1507, Nov. 1996, https://doi.org/10.1016/0021-9290(96)84547-7.

[41] M. Baniasad, F. Farahmand, M. Arazpour, and H. Zohoor, "Coordinated activities of trunk and upper extremity muscles during walker-assisted paraplegic gait: A synergy study," *Human Movement Science*, vol. 62, pp. 184-193, Dec. 2018, https://doi.org/10.1016/j.humov.2018.10.002.

[42] S. L. Delp, F. C. Anderson, A. S. Arnold, P. Loan, A. Habib, C. T. John, E. Guendelman, and D. G. Thelen, "OpenSim: open-source software to create and analyze dynamic simulations of movement," *IEEE transactions on biomedical engineering*, vol. 54, no. 11, pp.1940-1950, Oct. 2007, https://doi.org/10.1109/TBME.2007.901024.

[43] R. Drake, A. Vogl Wayne, , R. Tibbitts, and P. Richardson, Gray's Atlas of Anatomy E-Book. Elsevier Health Sciences, 2020.

[44] S. Nakamura, R. D. Crowninshield, and R. R. Cooper, "An analysis of soft tissue loading in the foot--a preliminary repor," *Bulletin of Prosthetics Research*, vol. 10, pp. 27-34, Jan 1981, https://www.rehab.research.va.gov/jour/81/18/1/pdf/nakamura.pdf.

[45] M. Zhang and A. F. T. Mak, "In vivo friction properties of human skin," *Prosthetics and Orthotics International*, vol. 23, no. 2, pp. 135–141, Aug. 1999, https://doi.org/10.3109/03093649909071625.

[46] Z.-H. Qian, L. Ren, L.-Q. Ren, and A. Boonpratatong, "A Three-Dimensional Finite Element Musculoskeletal Model of the Human Foot Complex," *IFMBE Proceedings 6th World Congress of Biomechanics (WCB 2010). August 1-6, 2010 Singapore*, pp. 297–300, 2010, https://doi.org/10.1007/978-3-642-14515-5_77.

[47] J. T.-M. Cheung, M. Zhang, A. K.-L. Leung, and Y.-B. Fan, "Three-dimensional finite element analysis of the foot during standing—a material sensitivity study," *Journal of Biomechanics*, vol. 38, no. 5, pp. 1045–1054, May 2005, https://doi.org/10.1016/j.jbiomech.2004.05.035.

[48] C. Mkandawire, W. R. Ledoux, B. J. Sangeorzan, and R. P. Ching, "Foot and ankle ligament morphometry," *Journal of Rehabilitation Research & Development*, vol. 42, no. 6, Nov. 2005, https://doi.org/10.1682/jrrd.2004.08.0094.

[49] D. W.-C. Wong, W. Niu, Y. Wang, and M. Zhang, "Finite Element Analysis of Foot and Ankle Impact Injury: Risk Evaluation of Calcaneus and Talus Fracture," *PLOS ONE*, vol. 11, no. 4, p. e0154435, Apr. 2016, https://doi.org/10.1371/journal.pone.0154435.

[50] S. A. Roelker, E. J. Caruthers, R. K. Hall, N. C. Pelz, A. M. Chaudhari, and R. A. Siston, "Effects of Optimization Technique on Simulated Muscle Activations and Forces," *Journal of Applied Biomechanics*, vol. 36, no. 4, pp. 259–278, Aug. 2020, https://doi.org/10.1123/jab.2018-0332.

[51] U. Trinler, H. Schwameder, R. Baker, and N. Alexander, "Muscle force estimation in clinical gait analysis using AnyBody and OpenSim," *Journal of Biomechanics*, vol. 86, pp. 55–63, Mar. 2019, https://doi.org/10.1016/j.jbiomech.2019.01.045 .

[52] K. E. Chatwin, C. A. Abbott, A. J. M. Boulton, F. L. Bowling, and N. D. Reeves, "The role of foot pressure measurement in the prediction and prevention of diabetic foot ulceration—A comprehensive review," *Diabetes/Metabolism Research and Reviews*, vol. 36, no. 4, Dec. 2019, https://doi.org/10.1002/dmrr.3258 .

[53] A. M.Galea, K. Springett, H. Bungay, S. Clift, S. Fava, and M. Cachia, "Incidence and location of diabetic foot ulcer recurrence," *Diabet Foot J*, vol. 12, no. 4, pp. 181-6, Dec. 2009.

[54] P. Pit'hová, H. Patkova, I. Galandakova, L. Dolezalova, and M. Kvapil, "Differences in ulcer location in diabetic foot syndrom," *Vnitrni lekarstvi*, vol. 53, no. 12, p. 1278, Dec. 2007.

[55] D. G. Armstrong, and L. A. Lavery, "Diabetic foot ulcers: prevention, diagnosis and classification." *American family physician*, vol. 57, no. 6, p. 1325, Mar. 1998.

[56] M. J. Mueller, S. D. Minor, J. E. Diamond, and V. P. Blair, "Relationship of Foot Deformity to Ulcer Location in Patients with

Diabetes Mellitus," *Physical Therapy*, vol. 70, no. 6, pp. 356–362, Jun. 1990, 10.1093/ptj/70.6.356, https://doi.org/10.1093/ptj/70.6.356.

[57] S. A. Bus, M. Maas, A. de Lange, R. P. Michels, & M. Levi, "Elevated plantar pressures in neuropathic diabetic patients with claw/hammer toe deformity," *Journal of biomechanics*, vol. 38, no. 9, pp. 1918-1925, Sep. 2005, https://doi.org/10.1016/j.jbiomech.2004.07.034.

[58] X. Yu, G. R. Yu, Y. X. Chen, X. C. Liu, "The characteristics and clinical significance of plantar pressure distribution in patients with diabetic toe deformity: a dynamic plantar pressure analysis," *Journal of International Medical Research*, vol. 39, no. 6, pp.2352-2359, Dec. 2011, https://doi.org/10.1177/147323001103900635.

[59] K. J. Mickle, B. J. Munro, S. R. Lord, H. B. Menz, J. R. Steele, "Gait, balance and plantar pressures in older people with toe deformities," *Gait & posture*, vol. 34, no. 3, pp. 347-351, Jul. 2011, https://doi.org/10.1016/j.gaitpost.2011.05.023.

[60] A. M. Galica, T. J. Hagedorn, A. B. Dufour, J. L. Riskowski, H. J. Hillstrom, V. A. Casey, & M. T. Hannan, "Hallux valgus and plantar pressure loading: the Framingham foot study," *Journal of foot and ankle research*, vol. 6, no. 1, pp.1-8, Dec. 2013, https://doi.org/10.1186/1757-1146-6-42.

Highlights

Re: A structural investigation of the internal stresses of the foot in hammer toe deformity during walking: A finite element approach, by: M. Moayedi, A. R. Arshi, M. Salehi*, M. Akrami, and R. Naemi

Manuscript reference No.: CIBM-D-21-00782

We developed a 3D finite element modeling of the foot with hammer toe deformity.

Gait analysis, musculoskeletal modelling, and electromyography test were utilised.

Predicted internal stresses in the soft tissue were found to be 1.64 greater than plantar pressure.

Maximum internal stresses in the hard tissue were observed at the 3rd and 5th metatarsals.

Hammer toe shifts the location of maximum stresses to the forefoot and raises the risk of ulcers

Appendix A:

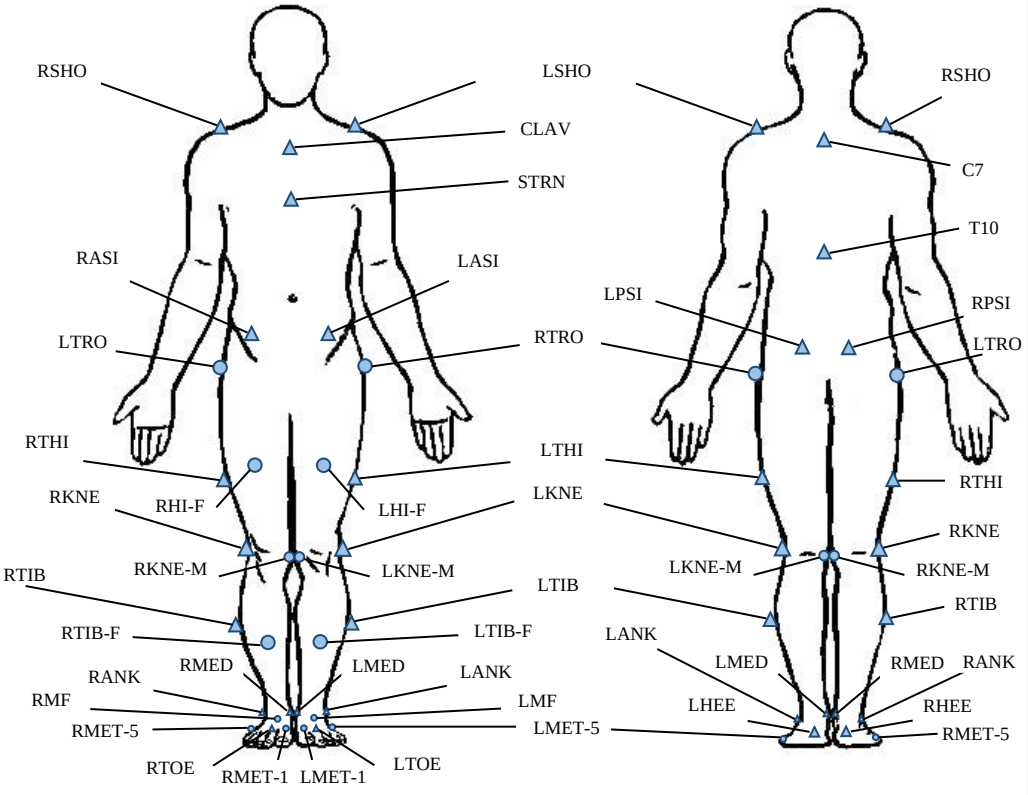

Description of the 24 markers placed based on Plug-in Gait standard [34]:

- Left & right shoulder (LSHO & RSO) on the acromioclavicular joint
- Clavicle (CLAV), on where the clavicles meet the sternum
- Sternum (STRN), on the xiphoid process
- C7 (7th cervical vertebra)
- T10 (10th thoracic vertebra)
- Left & right anterior superior iliac spine (LASI & RASI)
- Left & right posterior superior iliac spine (LPSI & RPSI)
- Left & right thigh, over the lower 1/3 of the thigh (LTHI & RTHI)
- Left & right knee, over the lateral femoral condyle (LKNE & RKNE)
- Left & right tibia, over the upper 1/3 of the shank (LTIB & RTIB)
- Left & right medial malleolus (LMED & RMED)
- Left & right ankle (LANK & RANK) on the lateral malleolus
- Left & right second toe metatarsal head (LTOE & RTOE)
- Left & right heel (LHEE & RHEE), on the calcaneus at the same height of LTOE (RTOE) marker

Description of the 14 extra markers placed based on previous studies [35-38]

- Left & right protrusive point of the greater trochanter (LTRO & RTRO)
- Left & right first metatarsal head (LMET-1 & RMET-1)
- Left & right fifth metatarsal head (LMET-5 & RMET-5)
- Left & right medial femoral condyle (LKNE-M & RNKE-M)
- Left and right dorsal surface of the second metatarso-cuneiform joint (LMF & RMF)

Left & right anterior tibia (LTIB-F & RTIB-F), at the half of part length

Left & right anterior thigh (LTHI-F & RTHI-F), at the half of part length

Fig. A1. Body marker set. The triangles represent markers placed based on Plug-in Gait standard [34], and the circles indicates extra markers positioned based on previous studies [35-38].

Appendix B:

For more details of stress distribution in bony structures, each phase shows with separate contour.

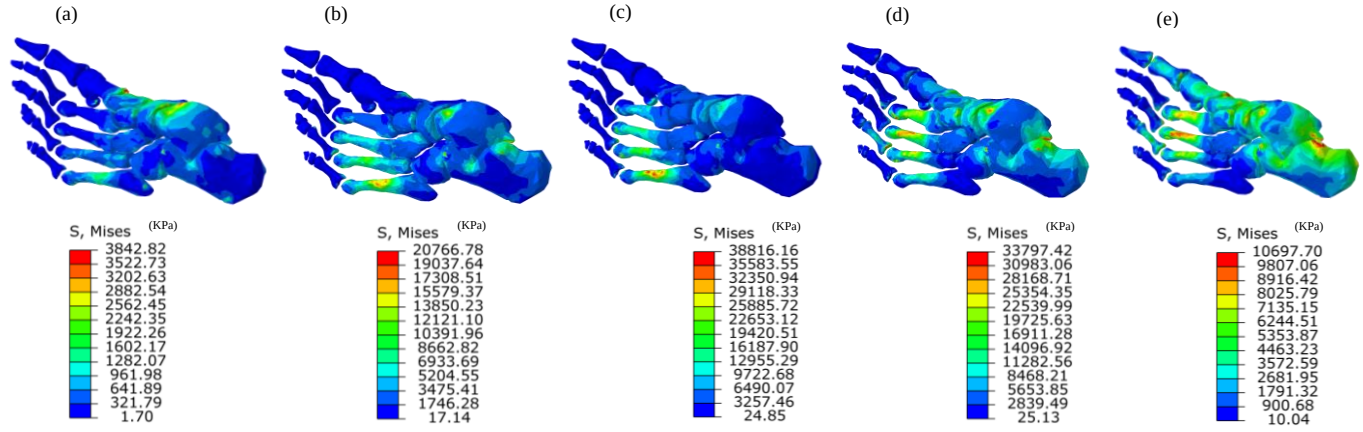

Fig. B1. Finite element internal stresses in bones at five walking events: (a) Heel strike (b) Early stance, (c) Mid-stance, (d) Late stance and (e) Toe off.